Enzyme and Microbial Technology 121 (2019) 23–28

Contents lists available at ScienceDirect

Enzyme and Microbial Technology

journal homepage: www.elsevier.com/locate/enzmictec

Modeling of an electrochemical nanobiosensor in COMSOL Multiphysics to determine phenol in the presence of horseradish peroxidase enzyme

Amir Kaffash[a], Khosrow Rostami[a,*], Hamid R. Zare[b,*]

[a] Department of Biotechnology, Iranian Research Organization for Science and Technology, 13815-3538, Tehran, Iran
[b] Department of Chemistry, Yazd University, Yazd, 89195-741, Iran

ARTICLE INFO

Keywords:
Horseradish peroxidase
Phenol determination
Electrochemical nanochip
Modeling
COMSOL Multiphysics

ABSTRACT

Horseradish peroxidase enzyme selectively oxidizes phenol to *o*-quinone that can be reduced electrochemically to catechol and generating a current response which is directly proportional to phenol concentration. In order to investigate the *o*-quinone enzymatic production and its electrochemical behavior, a 2-D model was developed for a nanochip biosensor in COMSOL Multiphysics. The oxidation rate of phenol to *o*-quinone was predicted by the developed model based on Michaelis-Menten equation. The diffusion coefficient of *o*-quinone was obtained 2.17×10^{-6} cm^2 s^{-1} based on experimental chronoamperograms. The cathodic and anodic peak potentials for *o*-quinone/catechol redox couple are obtained experimentally 255 and 310 mV, respectively. The obtained results from simulation were compared with the experimental results to verify the validity of the model. By comparing the cyclic voltammograms from the simulation and experimental results, the heterogeneous rate constant, k°, and the transfer coefficient, α, were calculated 0.02 cm s^{-1} and 0.5, respectively. Then, using simulation results, chronoamperograms were drawn for the nanochip biosensors with different heights. Also, *o*-quinone concentration gradients were determined at the electrode surface, which can be used to estimate the thickness of the diffusion layer. Finally, a calibration plot was obtained based on the simulation results of the proposed nanochip as phenol biosensor with the following equation I (nA) = 0.1497 C (μM)–0.3521 and a linear range of 20.0–150.0 μM.

1. Introduction

Phenol is a serious threat to environment and human health and it is reported as a priority pollutant in many countries. Phenol is commonly present in different industries wastewater such as petrochemicals, plastics, dyes, drugs, paper, pesticides, and textiles. Therefore, it is crucial to develop sensing systems in order to control phenol in water samples [1,2]. The electrochemical biosensors as promising tools are applied for phenol analyses since the method is selective, sensitive, reliable, easy to use, and inexpensive [3–5]. Moreover, miniaturizing electrochemical cells offer an excellent potential for biosensing applications with higher sensitivity, easier operation, lower cost, and less consumption of reagents [6,7].

Nowadays, computer modeling and simulation have been an essential part of science and engineering for development and optimization of devices. Mathematical models provide a lot of information that can maximize physical insight and predictive power for designing and improving devices such as sensors and biosensors [8–10]. Jin et al. [4] developed a model for nanoparticles based on amperometric glucose biosensor that suggests opportunities for designing complex integrated circuits of different sensors. Caussen et al. [11] evaluated a glucose biosensor model for optimization of spatial arrangement of platinum nanosphere and single wall carbon nanotube. Inoue et al. [3] modeled a screen-printed endotoxin sensor to investigate the influence of electrochemical cell geometry on the amperometric signals. Popovtzer et al. [12] presented a mathematical model for a phenol biosensor in a miniaturized electrochemical cell that can be used in similar systems with different geometries, materials and biological components. Baronas et al. [13] developed mathematical model of an enzyme electrode to understand the influence of substrate concentration, enzymatic rate, and membrane thickness on the biosensor amperometric responses.

In the present study, from experimental results, the diffusion coefficient and redox potential of *o*-quinone which is produced from phenol enzymatic oxidation were calculated. Then, a two dimensional (2-D) model was developed for a nanochip using finite element (FEM) software COMSOL Multiphysics (ver. 5.2, COMSOL, Inc., MA, USA) to study the electrochemical behavior of *o*-quinone in the nanochip biosensor. Also, the enzymatic reaction rate of phenol to *o*-quinone was

* Corresponding authors.
E-mail addresses: rostami@irost.ir (K. Rostami), hrzare@yazd.ac.ir (H.R. Zare).

https://doi.org/10.1016/j.enzmictec.2018.11.001
Received 17 July 2018; Received in revised form 1 November 2018; Accepted 1 November 2018
Available online 03 November 2018
0141-0229/

studied by numerical simulation and the results were compared with the experimental observations.

2. Materials and methods

2.1. Experimental

Horseradish peroxidase enzyme (HRP) was supplied from Sigma-Aldrich Company and hydrogen peroxide (30%, w/v aqueous solution), phenol, and all the other chemicals were purchased from Merck Company. The electrochemical measurements were performed by a PGSTAT101 and a three-electrode system. The experiments were performed in a 0.1 M phosphate buffer solution (PBS) containing HRP enzyme and different concentrations of H_2O_2 and phenol. A glassy carbon electrode (GCE) was used as the working electrode, a saturated calomel electrode (SCE) and a platinum electrode acted as the reference and the counter electrodes, respectively.

2.2. Reactions and governing equations

The enzymatic oxidation of phenol to electroactive *o*-quinone occurs in three steps. First, HRP in the presence of H_2O_2 is converted to a highly oxidative compound I (reaction 1). Then, compound I can easily oxidize phenol to phenoxyradical that immediately and selectively converts to *o*-quinone which is an electroactive species (reactions 2 and 3) [14–16].

$$H_2O_2 + HRP \xrightarrow{k_1} \text{compound I} + H_2O \quad (1)$$

$$\text{Phenol} + \text{compound I} \xrightarrow{k_2} o-\text{quinone} + \text{compound II} \quad (2)$$

$$\text{Phenol} + \text{compound II} \xrightarrow{k_3} o-\text{quinone} + HRP \quad (3)$$

The reactions (1)–(3) can be combined to yield reaction (4).

$$H_2O_2 + 2\ \text{phenol} \xrightarrow{HRP} 2o-\text{quinone} + H_2O \quad (4)$$

The produced *o*-quinone undergoes a reversible reduction to catechol at the electrode surface as explained in reaction (5). The measured electrochemical current attributed to the *o*-quinone reduction through reaction (5) which is proportional to the concentration of *o*-quinone and is directly related to phenol concentration [5,14,15].

$$o\text{-Quinone} + 2H^+ + 2e^- \leftrightarrows \text{Catechol} \quad (5)$$

Reaction (4) explains the enzymatic oxidation of phenol which occurs in the solution while reaction (5) is an electrochemical reaction. The Michaelis-Menten model can be used to determine *o*-quinone production rate (reaction 4) and its concentration in the solution. Based on this model, the reaction rate is calculated as follows [17]:

$$V = \frac{V_{max}\,[S]}{K_m + [S]} \quad (6)$$

where V is the reaction rate, [S] is the substrate concentration, V_{max} is maximum rate of reaction and K_m is Michaelis-Menten constant. The application of this frame for two-substrate enzymatic reaction is expressed as Eq. (7) in which V_{max} is k_3[HRP][phenol], K_m is k_3/k_1[phenol] and k_1 and k_3 are the rate constants of reactions (1) and (3) [17,18]:

$$V = \frac{k_3\,[HRP][phenol][H_2O_2]}{\frac{k_3}{k_1}[phenol] + [H_2O_2]} \quad (7)$$

Using this model, the concentration of *o*-quinone in solution, which undergoes electrochemical process in reaction (5), is calculated. The electrochemical response of the biosensor is proportional to the mass transfer of *o*-quinone molecules toward the working electrode if *o*-quinone reduction is diffusion-controlled. Generally, the diffusion of species i from bulk solution to the electrode is described by Fick's first and second laws [19];

$$J_i(x) = -D_i \frac{\partial C_i(x)}{\partial x} \quad (8)$$

$$\frac{\delta C_i}{\delta t} = -D_i \frac{\partial^2 C_i(x)}{\partial x^2} \quad (9)$$

where $J_i(x)$ is the diffusion flux of species i in x direction and D_i is diffusion coefficient of species i in bulk solution. If the electrochemical reaction is controlled by diffusion and electron transfer kinetics, Butler-Volmer equation is used for evaluation of cyclic voltammograms which is expressed as [19]:

$$i = nFAk^0\left[C_{ox}(0,t)\exp(-\alpha\frac{F}{RT}(E - E^{0'}) - C_{red}(0,t)\exp((n-\alpha)\frac{F}{RT}(E - E^{0'}))\right] \quad (10)$$

where n is the number of transferred electrons, F is Faraday's constant, A is electrode surface area, k° is the standard heterogeneous rate constant of the reaction, α is the cathodic transfer coefficient and $E^{0'}$ is the standard potential of a redox couple [19].

2.3. Geometry and assumptions

In the present study, a nano electrochemical cell was considered in order to investigate the electrochemical behavior of *o*-quinone which is produced from the phenol enzymatic oxidation. The geometry of the proposed cell is introduced in Scheme 1A. It illustrates the 3-D design of the chip with working electrode on its surface. These types of nanochips with embedded electrodes are frequently used in electrochemical biosensing applications [3,20,21]. For numerical calculations, a vertical cross section of this nanochip was selected as 2-D simulation domain. 2-D modeling is commonly reported in other electrochemical simulation studies that results to increase computational speed with reduced memory requirements [3,22–24]. As illustrated in Scheme 1B, the domain was meshed using free triangular type with extra fine element size. In the regions near the electrode surface, extremely fine mesh type with maximum 1.0 μm element size was used to make sure the convergence was reached.

The simulation process was divided into two time periods. In the first time period, the enzymatic reactions took place and the phenol was converted to *o*-quinone according to reaction (4). In the second time period, the electrochemical reduction of the electroactive *o*-quinone, which was generated by the preceding enzymatic reaction, was studied. The constants related to the enzymatic reactions of HRP and phenol were reported in the literature as $k_1 = 4.14 \times 10^5\ M^{-1}\ s^{-1}$ and $k_3 = 5.54 \times 10^4\ M^{-1}\ s^{-1}$ [18]. These constants were used for calculation of V_{max} and K_m. Also, molecular drift and convection in the cell were neglected since the solution in the measurement time is static.

2.4. Initialization and boundary conditions

As mentioned, the simulation comprises enzymatic process in the solution and the electrochemical reaction at the electrode surface. The concentrations of phenol, H_2O_2, and HRP at the beginning of enzymatic process were known and their concentration profiles were obtained based on Eq. (7). After enzymatic reaction in the solution was accomplished, it was assumed to be the starting point (t = 0) for electrochemical process simulation. Thus, the initial condition for electrochemical process was expressed as:

$$C_{o\text{-quinone}}(x, y, 0) = [o\text{-quinone produced in enzymatic reaction}] \quad (11)$$

In the electrochemical reaction, the reduction of *o*-quinone to catechol occurred at the electrode surface as described in reaction (5). This could be explained as a boundary condition in the electrochemical process.

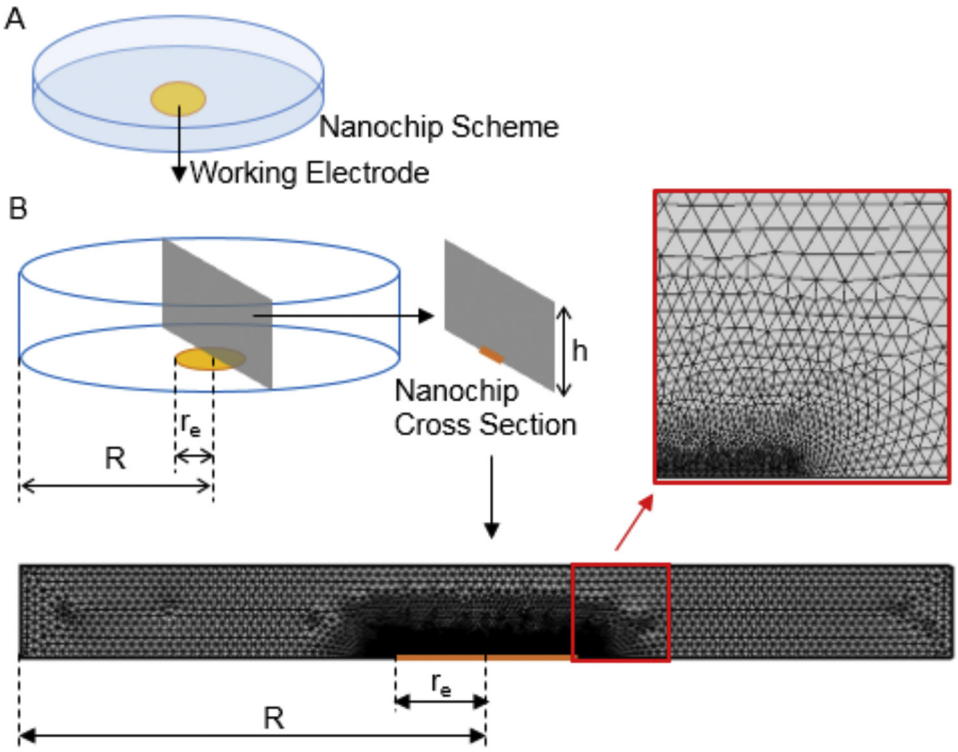

Scheme 1. (A) Schematic design of the simulated nanochip biosensor. (B) The detailed information of nanochip and the generated mesh for the 2-D domain of the nanochip cross section and its zoomed view.

$$C_{o\text{-quinone}}\ (x, 0, t) = 0.0 \text{ for } (x < r_e) \quad (12)$$

where r_e is the electrode radius.

3. Results and discussion

3.1. Diffusion coefficient

In order to calculate the diffusion coefficient of enzymatically generated *o*-quinone, chronoamperograms of the GCE in 10.0 mL solution of 0.1 M PBS (pH 7.0) containing H_2O_2, HRP enzyme and different concentrations of phenol at a potential step of 255 mV were obtained (Fig. 1). This potential step is sufficient to ensure that *o*-quinone reduction is diffusion-controlled [14]. For an electroactive species with a diffusion coefficient of D, the current response under diffusion-controlled process is described by Cottrell equation [19]:

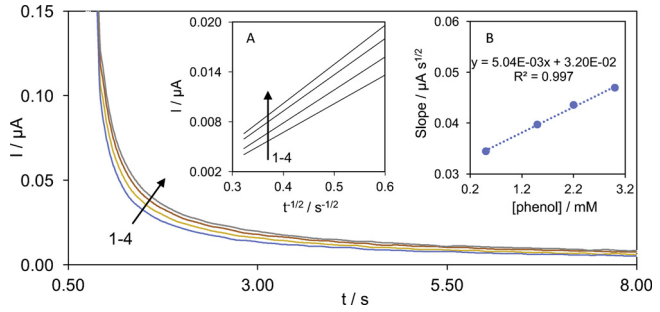

Fig. 1. Chronoamperometric responses of GCE in a 0.1 M phosphate buffer solution (pH 7.0) containing different concentrations of phenol and H_2O_2 at a potential step of 255.0 mV. Numbers 1–4 correspond to 0.5–3.0 mM phenol concentration. Insets: (A) plots of I vs. $t^{-1/2}$ obtained from chronoamperograms and (B) plot of the slope of straight lines of inset (A) vs. the phenol concentrations.

$$I = \frac{nFAD^{0.5}C}{\pi^{0.5} t^{0.5}} \quad (13)$$

Based on the Cottrell equation, the plot of I versus $t^{-1/2}$ is linear for different concentrations of phenol as shown in Fig. 1A. The slopes of the resulting straight lines were then plotted against the concentration of phenol as illustrated in Fig. 1B. According to the results and using the Cottrell equation, an experimental diffusion coefficient of 2.17×10^{-6} cm^2 s^{-1} was calculated. The diffusion coefficient plays a key role in the electrochemical response of an electroactive species.

3.2. Optimal conditions

In order to optimize the experimental conditions, the effect of buffer pH, phenol/H_2O_2 concentration ratio and enzyme concentration on the voltammetric responses was investigated. In all the experiments, the cyclic voltammograms of a GCE in a 0.1 M PBS containing phenol, H_2O_2 and HRP enzyme were recorded, and the reduction peak of *o*-quinone was used as a criterion for optimization. The maximum response for *o*-quinone reduction peaks was obtained at pH 7.0 as demonstrated in Fig. 2A. For higher and lower pH, the electrochemical responses decreased due to lower enzyme activity. In order to obtain the optimum concentration ratio of phenol/H_2O_2, the reduction peaks of *o*-quinone for the different ratios of 100.0/200.0, 100.0/100.0 and 100.0/50.0 of phenol/H_2O_2 (μM/μM) were compared in Fig. 2B. The best result was obtained for phenol/H_2O_2 ratio of 100.0 μM/100.0 μM. The lower concentration of H_2O_2 caused a decrease in *o*-quinone peak current that indicates the enzymatic reaction is not complete. Also, the higher concentration of H_2O_2 leaded to a decrease in reduction current that can be related to HRP inactivation by extra H_2O_2 in the solution [25]. The effect of HRP enzyme concentration in the solution in Fig. 2C indicated that 1.5 μM is an optimum concentration for phenol oxidation reaction to complete.

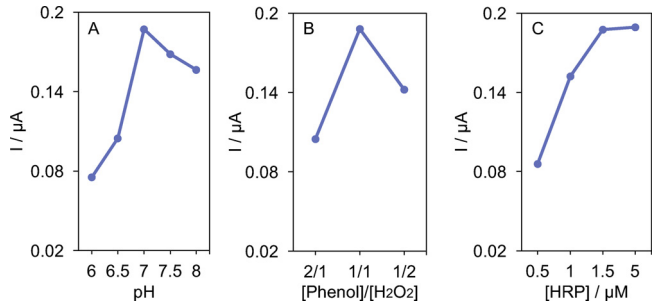

Fig. 2. (A) Effect of pH on reduction peaks in 0.1 M phosphate buffer solution containing 0.1 mM phenol, 0.1 mM H_2O_2 and 1.5×10^{-3} mM HRP enzyme. (B) Effect of concentration ratios of 100.0/200.0, 100.0/100.0 and 100.0/50.0 phenol/H_2O_2 (μM/μM) on reduction peaks in 0.1 M phosphate buffer solution. (C) Effect of HRP enzyme concentration on reduction peaks in 0.1 M phosphate buffer solution containing 0.1 mM phenol and 0.1 mM H_2O_2.

3.3. Numerical implementation

In this part, the concentration profiles of the reactants and products (phenol, H_2O_2 and *o*-quinone) related to enzymatic process were achieved by the developed model in COMSOL Multiphysics. The concentration profiles of phenol and *o*-quinone depending on the enzymatic reaction rate were obtained from Michaelis-Menten model as Eq. (7). As it can be seen in Fig. 3A, the production of *o*-quinone was fulfilled in 30 s for initial concentrations of 0.1 mM phenol, 0.1 mM H_2O_2 and 1.5×10^{-3} mM HRP enzyme. Also, the experimental cyclic voltammograms recorded after addition of HRP enzyme to substrates solution (Fig. 3B) indicated that the peak currents related to *o*-quinone reduction increased gradually during 30 s and reached to its final value as illustrated in Fig. 3A. Fig. 3C, voltammogram a, displays the cyclic voltammogram of GCE in 0.1 M PBS (pH 7.0) containing 0.1 mM phenol and 0.1 mM H_2O_2 in the absence of HRP enzyme in the potential range of 0.1–0.9 V. This voltammogram represented an anodic peak at E = 0.7 V which was attributed to phenol electrochemical oxidation.

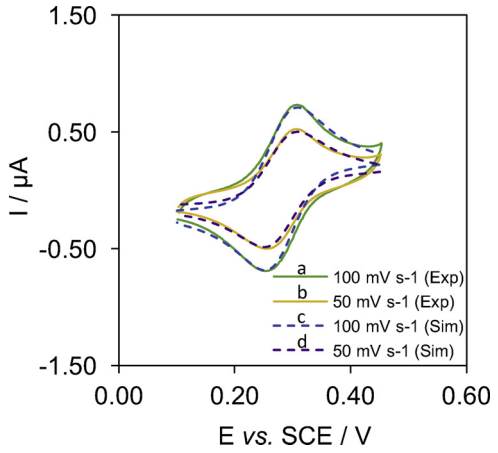

Fig. 4. Cyclic voltammograms of experimental (a, b) and theoretical (c, d) corresponding to a 0.1 M PBS (pH 7.0) containing 0.1 mM phenol, 0.1 mM H_2O_2 and 1.5×10^{-3} mM HRP enzyme in potential scan rates of 50.0 and 100.0 mV s^{-1}.

Voltammogram b of Fig. 3C is related to GCE in 0.1 M PBS (pH 7.0) containing 0.1 mM phenol and 0.1 mM H_2O_2 in presence of 1.5×10^{-3} mM HRP enzyme. This voltammogram showed a redox peak which was related to *o*-quinone/catechol redox couple [14]. In addition, no peak was observed for phenol oxidation in the potential range of 0.1–0.9 V. These results indicated that phenol was completely consumed in the presence of HRP enzyme. Therefore, for a solution containing 0.1 mM phenol, 0.1 mM H_2O_2 and 1.5×10^{-3} mM HRP enzyme, it was logical to consider $C_{o\text{-quinone}}$ equaled 0.1 mM as an initial condition of electrochemical process simulation.

After the enzymatic step was accomplished in 30 s, the voltammograms of the developed model in COMSOL Multiphysics were studied in order to gain a more precise insight on the electrochemical process. The experimental cyclic voltammograms (a) and (b) of Fig. 4 show the

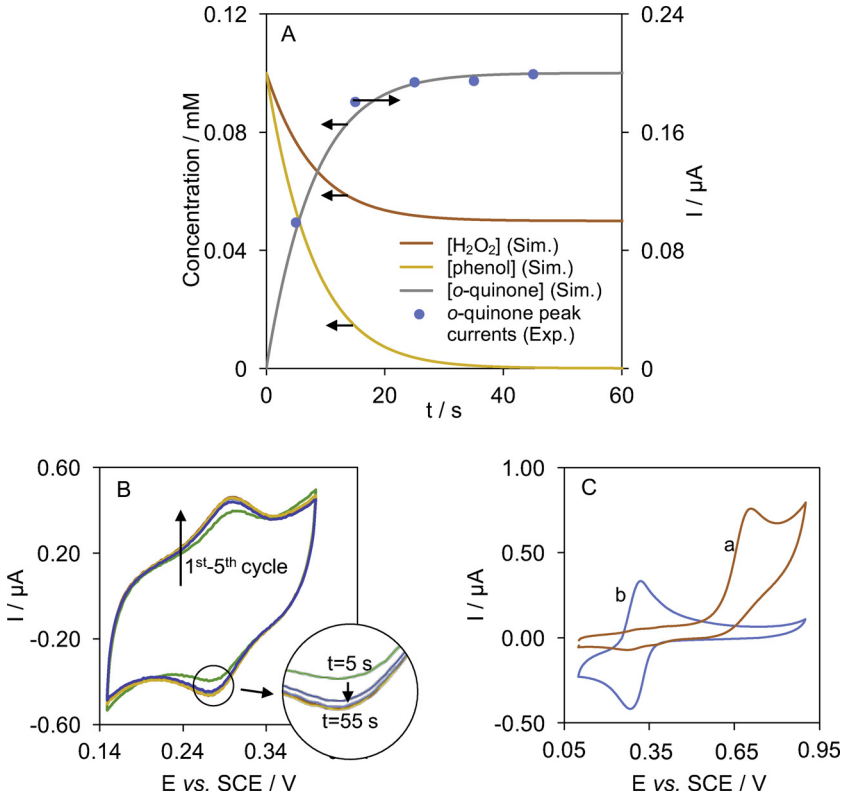

Fig. 3. (A) Simulation and experimental results for phenol, H_2O_2 and o-quinone concentration profiles related to a 0.1 M PBS (pH 7.0) with initial concentrations of 0.1 mM phenol, 0.1 mM H_2O_2 and 1.5×10^{-3} mM HRP enzyme. The dots show the cathodic peak currents of o-quinone reduction. These cathodic peak currents related to the experimental cyclic voltammograms that have been taken after mixing phenol, H_2O_2 and HRP enzyme over different time periods. (B) Five consecutive experimental cyclic voltammograms related to GCE in a 0.1 M PBS (pH 7.0) containing 0.1 mM phenol, 0.1 mM H_2O_2 and 1.5×10^{-3} mM HRP enzyme. Potential scan rate was 50.0 mV s^{-1}. (C) The cyclic voltammograms of GCE in a 0.1 M phosphate buffer solution (pH 7.0) containing (a) 0.1 mM phenol and 0.1 mM H_2O_2 in absence of HRP enzyme and (b) 0.1 mM phenol and 0.1 mM H_2O_2, 30.0 s after addition of HRP enzyme in the potential range of 0.1–0.9 V.

voltammograms of GCE in 10.0 mL of 0.1 M PBS (pH 7.0) containing 0.1 mM phenol, 0.1 mM H_2O_2 and 1.5×10^{-3} mM HRP enzyme after 30 s. The voltammograms (a) and (b) recorded at the potential scan rates of 50 and 100 mV s^{-1}, respectively, showed a redox pair that was attributed to the *o*-quinone reduction at 255 mV and catechol oxidation at 310 mV. Then, using the parameters evaluated from experimental data such as redox potentials and diffusion coefficient, the theoretical cyclic voltammograms for same geometry as experimental set-up were calculated based on Butler-Volmer equation. Also, the values of the unknown constants in Eq. (10), namely k° and α, were guessed. As it is demonstrated in Fig. 4, voltammograms (c) and (d), when the values of k° and α for *o*-quinone/catechol redox couple were assumed 0.02 cm s^{-1} and 0.5, respectively, the closest results to experimental voltammograms (a) and (b) were observed. Therefore, a good agreement between experimental results and simulation results suggests that the developed model can predict the electrochemical behavior of *o*-quinone in the proposed nanochip and provide much information about electrochemical responses without carrying out further experiments.

3.4. Voltammetric results of simulation

Based on experimental cyclic voltammograms (a) and (b) of Fig. 4, it was clear that, the reduction process of enzymatically generated *o*-quinone at potential step of 255 mV was a diffusion-controlled process. Thus, this potential step was applied to investigate diffusion-controlled reduction of *o*-quinone to catechol (reaction 5) in the nanochip model by COMSOL Multiphysics. The calculated chronoamperograms obtained for *o*-quinone reduction in the nanochip with different heights are shown in Fig. 5. The change in the height of the nanochip resulted to different chronoamperograms for *o*-quinone reduction. In order to explain the differences between simulated chronoamperograms, the concentration distribution of *o*-quinone, after 0.5, 2.0, 5.0, 10.0, 20.0 and 50.0 s from the potential step were calculated as illustrated in Fig. 6. At the beginning of electrochemical process, the *o*-quinone concentration was constant in whole domain of the designed nanochip. As it can be seen in Fig. 6, the reduction process of *o*-quinone to catechol leaded to the depletion of electroactive *o*-quinone near the electrode surface. The generated concentration gradient caused the diffusion of *o*-quinone from bulk solution to the electrode and thus, the diffusion layer gradually expanded to the bulk solution. Therefore, the calculated *o*-quinone reduction currents in chronoamperograms decreased as the diffusion layer expanded. Also, with changing the height of the nanochip biosensor from 300.0 to 50.0 μm, the maximum thickness of diffusion layer that can be expanded in the bulk solution

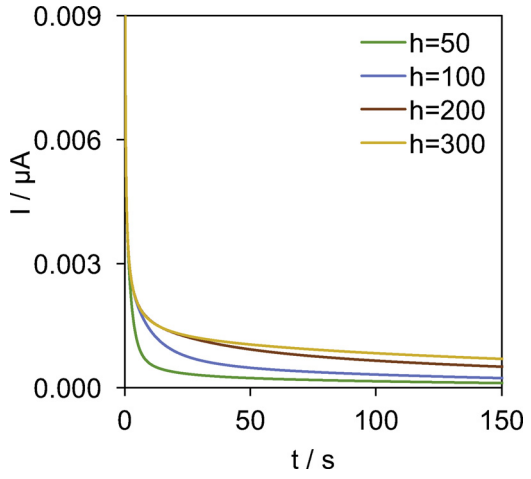

Fig. 5. Simulated chronoamperograms related to a nanochip with different heights (h). Electrode radius, r_e, and nanochip radius, R, were considered 100.0 μm and 500.0 μm, respectively.

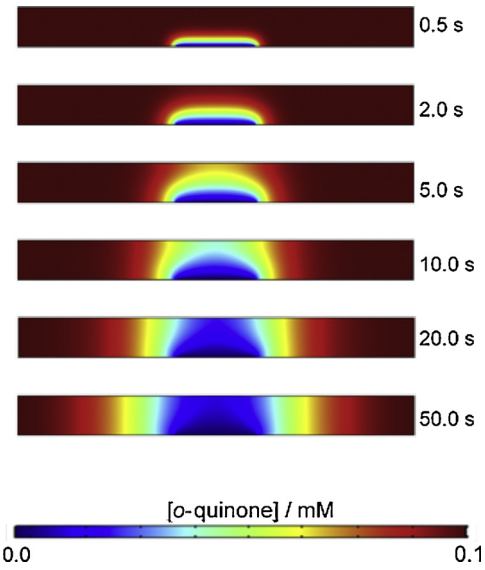

Fig. 6. The color maps of o-quinone concentarion gradients and the expansion of the diffusion layer after applying the potential step to the nanochip. Electrode radius (r_e), nanochip radius (R) and nanochip height (h) were considered 100.0 μm, 500.0 μm and 100.0 μm, respectively.

reduced and consequently the chronoamperometric response decrease with a greater slope. The results indicated that using the developed model, it is possible to calculate the values of k°, α and the changes in diffusion layer thickness during the time of a transient voltammetry method such as chronoamperometry.

In order to estimate the quantitative parameters of phenol determination by the proposed nanochip, simulated cyclic voltammetry responses were found under optimal conditions (Fig. 7A). The reduction peak currents of phenol enzymatic oxidation product, *o*-quinone, corresponding to the different concentrations of phenol were obtained from cyclic voltammograms of Fig.7A. Then, the *o*-quinone reduction peak currents were used to construct a calibration plot. As it is shown in Fig. 7B, a linear relationship was obtained for the proposed biosensor in the concentration range of 20.0–150.0 μM with the equation I (nA) = 0.1497 C (μM) - 0.3521, R^2 = 0.9966.

4. Conclusion

In the present study, a numerical model was developed to describe enzymatic reaction of phenol and horseradish peroxidase. The product of phenol enzymatic reaction is *o*-quinone that can be reduced electrochemically to catechol. The cathodic peak current was used to determine the phenol concentration in the analyte solution. The performed experiments for obtaining the optimal conditions indicated that the system is operative for phenol determination as an electrochemical biosensor. Using the proposed model, the concentration profiles of phenol, H_2O_2 and *o*-quinone have been successfully predicted. According to experimental and simulation results of cyclic voltammetric studies, k° and α were calculated for redox couple of *o*-quinone/catechol. The parameters of k° and α were used to predict the electrochemical behavior of *o*-quinone in the proposed nanochip. Using the simulation results of the biosensor, it is possible to obtain useful information about the diffusion layer and concentration gradients of *o*-quinone at the electrode surface. Also, the calibration curve for different concentrations of phenol was predicted by the model. Therefore, it was indicated the proposed nanochip for phenol determination can be used as a promising tool for further researches in this field.

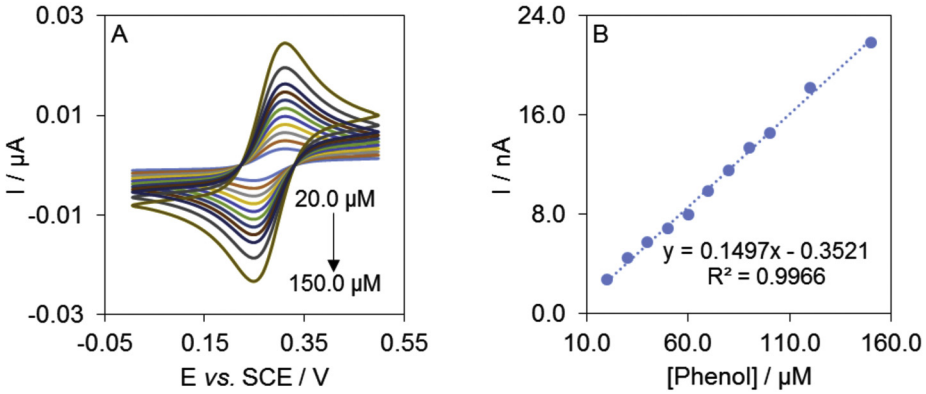

Fig. 7. (A) The simulated cyclic voltammograms corresponding to the different concentrations of phenol (20.0–150.0 μM). (B) Calibration plot of the reduction peak currents of phenol enzymatic oxidation product, o-quinone, vs. the concentration of phenol obtained from simulated cyclic voltammograms.

References

[1] F.R. Caetano, E.A. Carneiro, D. Agustini, L.C.S. Figueiredo-Filho, C.E. Banks, M.F. Bergamini, L.H. Marcolino-Junior, Combination of electrochemical biosensor and textile threads: a microfluidic device for phenol determination in tap water, Biosens. Bioelectron. 99 (2018) 382–388.

[2] N. Kolahchi, M. Braiek, G. Ebrahimipour, S.O. Ranaei-Siadat, F. Lagarde, N. Jaffrezic-Renault, Direct detection of phenol using a new bacterial strain-based conductometric biosensor, J. Environ. Chem. Eng. 6 (2018) 478–484.

[3] K.Y. Inoue, S. Takano, S. Takahashi, Y. Ishida, K. Ino, H. Shiku, T. Matsue, A screen-printed endotoxin sensor based on amperometry using a novel *p*-aminophenol conjugated substrate for a Limulus amebocyte lysate protease reaction, Analyst 138 (2013) 6523–6531.

[4] X. Jin, T.S. Fisher, M.A. Alam, Generalized compact modeling of nanoparticle-based amperometric glucose biosensors, IEEE Trans. Electron Devices 63 (2016) 4924–4932.

[5] R. Solná, P. Skládal, Amperometric flow-injection determination of phenolic compounds using a biosensor with immobilized laccase, peroxidase and tyrosinase, Electroanalysis 17 (2005) 2137–2146.

[6] X. Zhu, C.H. Ahn, On-chip electrochemical analysis system using nanoelectrodes and bioelectronic CMOS Chip, Sens. J. 6 (2006) 1280–1286.

[7] J.I. Hahm, Biomedical detection via macro- and nano-sensors fabricated with metallic and semiconducting oxides, J. Biomed. Nanotechnol. 9 (2013) 1–25.

[8] E.J. Dickinson, H. Ekström, E. Fontes, COMSOL Multiphysics: Finite element software for electrochemical analysis. A mini-review, Electrochem. Commun. 40 (2014) 71–74.

[9] M.W. Al-Mufti, U. Hashim, T. Adam, Simulation of nano lab on chip devices by using COMSOL Multiphysics, J. Appl. Sci. Res. 9 (2013) 1062–1066.

[10] R. Baronas, F. Ivanauskas, J. Kulys, Mathematical Modeling of Biosensors: an Introduction for Chemists and Mathematicians Vol. 9 Springer Science & Business Media, New York, 2009.

[11] J.C. Claussen, J.B. Hengenius, M.M. Wickner, T.S. Fisher, D.M. Umulis, D.M. Porterfield, Effects of carbon nanotube-tethered nanosphere density on amperometric biosensing: simulation and experiment, J. Phys. Chem. C 115 (2011) 20896–20904.

[12] R. Popovtzer, A. Natan, Y. Shacham-Diamand, Mathematical model of whole cell based bio-chip: an electrochemical biosensor for water toxicity detection, J. Electroanal. Chem. 602 (2007) 17–23.

[13] R. Baronas, J. Kulys, F. Ivanauskas, Modelling amperometric enzyme electrode with substrate cyclic conversion, Biosens. Bioelectron. 19 (2004) 915–922.

[14] A. Kaffash, H.R. Zare, K. Rostami, Highly sensitive biosensing of phenol based on adsorption of phenol enzymatic oxidation product on the surface of an electrochemically reduced graphene oxide-modified electrode, Anal. Methods 10 (2018) 2731–2739.

[15] Y. Zhang, J. Zhang, H. Wu, S. Guo, J. Zhang, Glass carbon electrode modified with horseradish peroxidase immobilized on partially reduced graphene oxide for detecting phenolic compounds, J. Electroanal. Chem. 681 (2012) 49–55.

[16] T.A. Enache, A.M. Oliveira-Brett, Phenol and para-substituted phenols electrochemical oxidation pathways, J. Electroanal. Chem. 655 (2011) 9–16.

[17] H. Ikemoto, Q. Chi, J. Ulstrup, Stability and catalytic kinetics of horseradish peroxidase confined in nanoporous SBA-15, J. Phys. Chem. C 114 (2010) 16174–16180.

[18] P.T. Vasudevan, L.O. Li, Kinetics of phenol oxidation by peroxidase, Appl. Biochem. Biotechnol. 60 (1996) 203–215.

[19] A.J. Bard, L.R. Faulkner, Electrochemical Methods: Fundamentals and Applications, 2th ed., Wiley, New York, 2001.

[20] R. Popovtzer, T. Neufeld, J. Rishpon, Y. Shacham-Diamand, Electrochemical detection of biological reactions using a novel nano-bio-chip array, Sens. Actuators B 119 (2006) 664–672.

[21] T. Neufeld, D. Biran, R. Popovtzer, T. Erez, E.Z. Ron, J. Rishpon, Genetically engineered pfabA pfabR bacteria: an electrochemical whole cell biosensor for detection of water toxicity, Anal. Chem. 78 (2006) 4952–4956.

[22] L. Cai, R.E. White, Mathematical modeling of a lithium ion battery with thermal effects in COMSOL Inc. Multiphysics software, J. Power Sources 196 (2011) 5985–5989.

[23] Y. Song, V. Penmatsa, C. Wang, Modeling and simulation of enzymatic biofuel cells with three-dimensional microelectrodes, Energies 7 (2014) 4694–4709.

[24] F. Song, N. Sridhar, A two-dimensional model for steel corrosion under a disbonded coating due to oxygen with or without cathodic protection—Part 1: Full numerical solution, Corrosion 62 (2006) 676–686.

[25] K.J. Baynton, J.K. Bewtra, N. Biswas, K.E. Taylor, Inactivation of horseradish peroxidase by phenol and hydrogen peroxide: a kinetic investigation, Biochim. Biophys. Acta. Protein Struct. Molec. Enzym. 1206 (1994) 272–278.